Thermodynamics of Formation, Reorganization, and Melting of Confined Nanometer-Sized Polymer Crystals

Andreas Röttele[†] and Thomas Thurn-Albrecht*

Fakultät für Physik, Albert-Ludwigs-Universität Freiburg, Hermann-Herder-Strasse 3, 79104 Freiburg, Germany

Jens-Uwe Sommer and Günter Reiter

Institut de Chimie des Surfaces et Interfaces, CNRS-UHA, 15, rue Jean Starcky, B.P. 2488, 68057 Mulhouse Cedex, France

Received September 5, 2002

ABSTRACT: We studied the thermodynamic properties of a large ensemble of polymer crystals confined in the spherical cells of a block copolymer mesostructure. Nucleated only at large supercoolings, the resulting highly imperfect crystallites showed significant reorganization upon heating. A broad melting range is caused by the superposition of sharp melting transitions of the individual crystals, which take place at different temperatures corresponding to a multitude of possible metastable states. Thus, at the limit of their stability, individual nanocrystals only have the choice between complete melting or stabilization by reorganization taking place entirely in the crystalline state. As a consequence of their smallness, melting−recrystallization processes within the individual cells are prohibited.

Introduction

In a polymer melt, individual chains acquire coiled states of high conformational entropy. During crystallization these chain molecules transform to low-entropy folded states.[1−3] Since complete stretching of long chains is extremely improbable, this process leads to nonequilibrium, highly imperfect structures.[4,5] Moreover, crystalline−amorphous superstructures on various length scales are generated, controlled by the kinetics of the crystallization process.[3] The resulting crystals are thus metastable: reorganization phenomena and a dependence of the melting point on thermal history are frequently observed.[3,4,6,7] This leads to a complex melting behavior which has often been interpreted in terms of a superposition of simple melting followed by a recrystallization of completely molten molecules below a postulated equilibrium melting point.[4,8,9]

To study the process of melting independent of recrystallization, we investigated nanometer-sized individual crystals separated by an amorphous matrix of a block copolymer mesostructure. The same system was recently studied in real space using tapping mode atomic force microscopy (AFM).[10] There, we found that nucleation is only possible at large supercooling of about 60 K and that growth of a crystal is effectively contained within one micellar unit of the mesostructure.

Here, we present a quantitative study of the thermodynamics of this system using ensemble averaging methods like calorimetry and X-ray scattering. In the interpretation of our data we take advantage of the detailed microscopic knowledge of the distribution of the crystals in the system gained previously by AFM. As we will show, the combination of direct space and ensemble averaged information greatly enhances the value of the macroscopic methods used and removes some possible ambiguity in their interpretation. In particular, we will show that the observed broad melting range is a consequence of a superposition of sharp melting points of the already existing individual crystals possessing different thermodynamic stability (crystalline order).

The thermodynamic forces driving crystallization are typically much larger than those acting in the soft ordered state of a block copolymer (large crystallization enthalpy). Therefore, the mesostructure of a block copolymer is easily changed upon crystallization.[11,12] However, in some cases it may be preserved (glassy matrix, strong segregation in highly asymmetric block copolymers, fast crystallization kinetics),[10,13−17] as it is the case in the system studied here. There are several ways how crystallization can be altered by the finite size of the system. As a very important effect, nucleation within each spherical compartment becomes the step dominating the overall crystallization kinetics in highly asymmetric diblock copolymers.[13,10,18,19] This concept has been introduced originally to describe the crystallization of droplets in emulsions.[20] We are effectively dealing with independent, individually formed small crystals whose properties can be strongly affected by the presence of interfaces.[21] In addition, chain conformations between the crystals and the amorphous matrix are coupled across the phase boundaries.[12] The stability (crystallinity) of the formed crystals, possible reorganization processes, and, in particular, the competition between such reorganization processes and final destruction (melting) of the crystals at relatively high temperatures will be examined in detail in this paper.

Experimental Section

We used hydrogenated poly(butadiene-*b*-ethylene oxide) (PB_h-*b*-PEO) with a molecular weight of the blocks of 21 100 and 4300 g/mol, respectively, corresponding to a PEO weight fraction of 17%. The PB_h block contains statistically distributed 1−4 and 1−2 units, with a majority (≈85%) of 1−2 units.[22] This block is therefore amorphous; it becomes glassy around $T_g \approx -18$ °C. The PEO block on the other hand can crystallize.

[†] Deceased.

* To whom correspondence should be addressed.

10.1021/ma021434c CCC: $25.00
Published on Web 01/25/2003

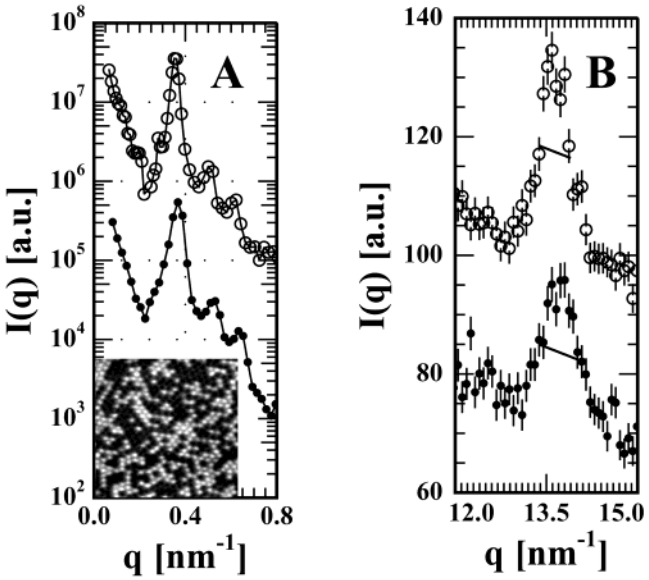

Figure 1. (A) Scattered intensity of PB_h-*b*-PEO as measured in a SAXS experiment in the amorphous state at $T = 130$ °C (open symbols, data shifted) and in the crystalline state at $T = 30$ °C (closed symbols). The microphase structure is identical for both states. The inset shows an AFM phase image of a partially crystalline sample (500 × 500 nm) after annealing for 2 min at 42 °C. The white and the dark circles represent crystalline and amorphous cells. (B) (120) Bragg reflection measured at $T = -40$ °C after crystallization (closed symbols) in comparison to a measurement at $T = 25$ °C taken from a relaxed sample (open symbols). The lateral size L of the crystals, based on a measure of the full width at half-maximum Δq of this peak,[27] is given by $L = 0.89 \times 2\pi/\Delta q$. After annealing around room temperature $\Delta q = 0.48$ nm^{-1}, corresponding to a crystal size of about 12 nm. This is consistent with the diameter of the cells containing these crystals as obtained from SAXS, i.e., 11.8 nm. In comparison, for a measurement taken at $T = -40$ °C shortly after crystallization, $\Delta q = 0.62$ nm^{-1}, corresponding to a crystal size of 9.0 nm.

The length of the fully extended crystalline PEO block is about 27 nm. In the temperature range of the experiment the block copolymer is microphase-separated. All samples were first annealed at $T \approx 140$ °C to obtain well-ordered microphase structures as starting condition. Small-angle X-ray scattering (SAXS) measurements were made on a Kratky compact camera using slit collimation. Data were desmeared using the algorithm developed by Strobl.[23] Wide-angle X-ray scattering experiments were performed on a Siemens D500 powder diffractometer equipped with a temperature-controlled sample stage. For calorimetric experiments a differential scanning calorimeter (Perkin-Elmer DSC 7) was used.

Results and Discussion

Highly asymmetric diblock copolymers form microphase structures consisting of micelles arranged on a body-centered-cubic (bcc) lattice.[3] Figure 1A shows two SAXS patterns of the polymer taken at $T = 130$ °C from an amorphous sample and at $T = 30$ °C from a crystalline sample. In both cases, the three peaks visible at relative positions of 1, $\sqrt{2}$, and $\sqrt{3}$ correspond to the (110), (200), and (211) reflections of the bcc lattice formed by PEO cells in a PB_h matrix. A detailed analysis of the measured structure factor[24] gives a lattice constant of 24.2 nm and a radius of 5.9 nm for the measurement at $T = 30$ °C. Thermal expansion leads to slightly higher values at the higher temperature. From these values a volume fraction of spheres of 12%, consistent with a weight fraction of 17%, follows. The materials contains 1.4×10^{17} PEO cells per cm^3; each cell consists of about 14200 monomers or 145 PEO blocks.

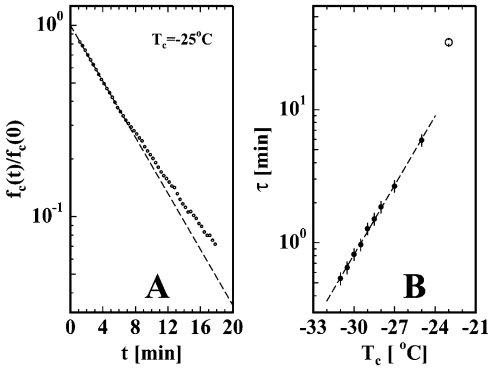

Figure 2. (A) Normalized rate of crystallization as measured by an isothermal DSC experiment at a temperature $T_c = -25$ °C. The initial slope in the semilogarithmic representation corresponds to the inverse time constant of crystallization $1/\tau$, giving $\tau = 6.6$ min. (B) Time constant τ of crystallization vs crystallization temperature T_c (DSC, filled symbols; AFM, open symbol).

Crystallization in this material happens only at high supercooling of about 60 K. This effect has been attributed to the high number of nuclei that are required for independent crystallization of every cell and that have to be formed by homogeneous nucleation.[13,10,18] As a consequence, nucleation becomes the rate-determining step. Data obtained from isothermal crystallization in DSC displaying this behavior are shown in Figure 2A. In a first approach, a simple exponential time law may be assumed: $f_c \propto \exp(-t/\tau)$. Here, f_c is the rate of crystallization, which is proportional to the measured heat flow. This approach fits well the data points for early stages of crystallization. However, deviations from such a simple exponential behavior were visible for the later stages. They could be attributed to the existence of some cells with a lower probability for crystallization.[10] The inverse time constant $1/\tau$ reflects the initial rate of nucleation. The time constant τ increased with increasing temperature (see Figure 2B).

Let us now turn to the calorimetric properties at crystallization and melting. The heat of crystallization ΔH_c, obtained by integrating the peak of crystallization as measured by DSC, amounts to 10 J/g. In a typical heating experiment as shown in Figure 3, the PEO crystals melt around $T_f \approx 45$ °C. The integrated area of the peak of fusion is denoted as the heat of fusion ΔH_f. For the experiment in Figure 3 we obtained $\Delta H_f \simeq 24$ J/g or 1.5×10^{-16} J/cell ($= 34 \times 10^3 k_B T$/cell). This value is more than 4 orders of magnitude larger than the typical energy of thermal fluctuations. Thus, our small crystals represent mesoscopic systems. Based on a comparison with the tabulated heat of fusion for PEO (197 J/g),[25] the internal crystallinity of a cell is about 72% (based on a PEO weight fraction of 17%). Remarkably, ΔH_c is considerably smaller than ΔH_f. Only part of this discrepancy can be explained by the normal temperature dependence of the enthalpy difference $\Delta H_c(T_c) = \Delta H_f(T_f) - \Delta H_{cf}(\Delta T)$ between the liquid and the crystalline state:

$$\Delta H_{cf} \approx \int_{T_c}^{T_f} [c_{p,l}(T) - c_{p,c}(T)]\, dT \qquad (1)$$

Here, $c_{p,l}$ and $c_{p,c}$ denote the extrapolated heat capacities of the liquid and the crystalline state.[26] For $T_c = -25$

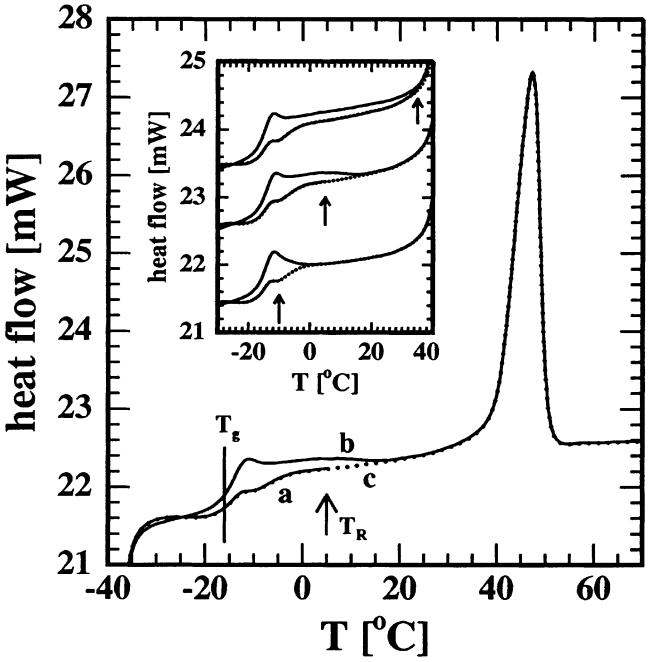

Figure 3. Reorganization processes taking place in the crystals during heating show up in DSC measurements by comparing melting runs with (b, solid line) and without (c, dotted line) a preceding annealing run (a). The annealing run (a, lower solid line) went up to a temperature $T_R = 5$ °C as indicated by the arrow. The two traces (b and c) do not overlap between $T \approx -25$ °C and $T \approx 15$ °C. The difference signal represents the exothermic contribution during heating without preceding annealing run in this temperature range. In the inset this part of the data is shown enlarged for $T_R = -10$ °C, $T_R = 5$ °C, and $T_R = 35$ °C (T_R is indicated by arrows). The temperature range over which the two signals differ depends on T_R. For all measurements heating rates of 10 K/min were used.

°C and $T_f = 42$ °C, $\Delta H_{cf}(\Delta T) \simeq 45$ J/g for pure PEO. Taking into account the weight fraction of PEO of 17% and the crystallinity of 72%, $\Delta H_{cf} \simeq 6$ J/g. Obviously, $\Delta H_{cf}(\Delta T)$ accounts only partially for the difference between ΔH_c and ΔH_f. There is still a discrepancy of 8 J/g. Energy conservation requires an additional contribution:

$$\Delta H_R = \Delta H_f - \Delta H_c - \Delta H_{cf}(\Delta T) \qquad (2)$$

Here, ΔH_R must result from an exothermic process during heating. We attribute this released energy ΔH_R to reorganization processes leading to improved crystalline states. These processes can be observed directly by DSC by performing adequate thermal cycles. An example is shown in Figure 3. A first heating run (a) up to a cutoff temperature $T_R = +5$ °C was performed directly after crystallization. During this run the sample was not melted, but reorganization was possible. The result of this reorganization was probed by a second heating run (b) immediately after the first one. The difference in signal between heating runs with (b) and without (c) a preceding annealing run (a) is a measure of the enthalpy gained during the annealing run (a) due to reorganization leading to improvement of the crystalline structure. Closer analysis shows that the additional exothermic signal as obtained by taking the integral over the difference of the two DSC runs depends on the temperature T_R. For the highest temperature $T_R = 35$ °C, it amounts to about 7 J/g, a value consistent with the expected value for ΔH_R of 8 J/g. Heating after a preceding annealing run also makes the glass transition ($T_g \approx -18$ °C) of the matrix clearly visible in the DSC trace (b). For nonrelaxed samples, the corresponding endothermic steplike increase in the heat capacity is masked by the opposing exothermic contribution caused by reorganization (crystal improvement) which sets in markedly in this temperature range. Obviously, crystal improvement requires a certain mobility of the surrounding matrix. The calorimetric observations can directly be related to WAXS observations (Figure 1B)

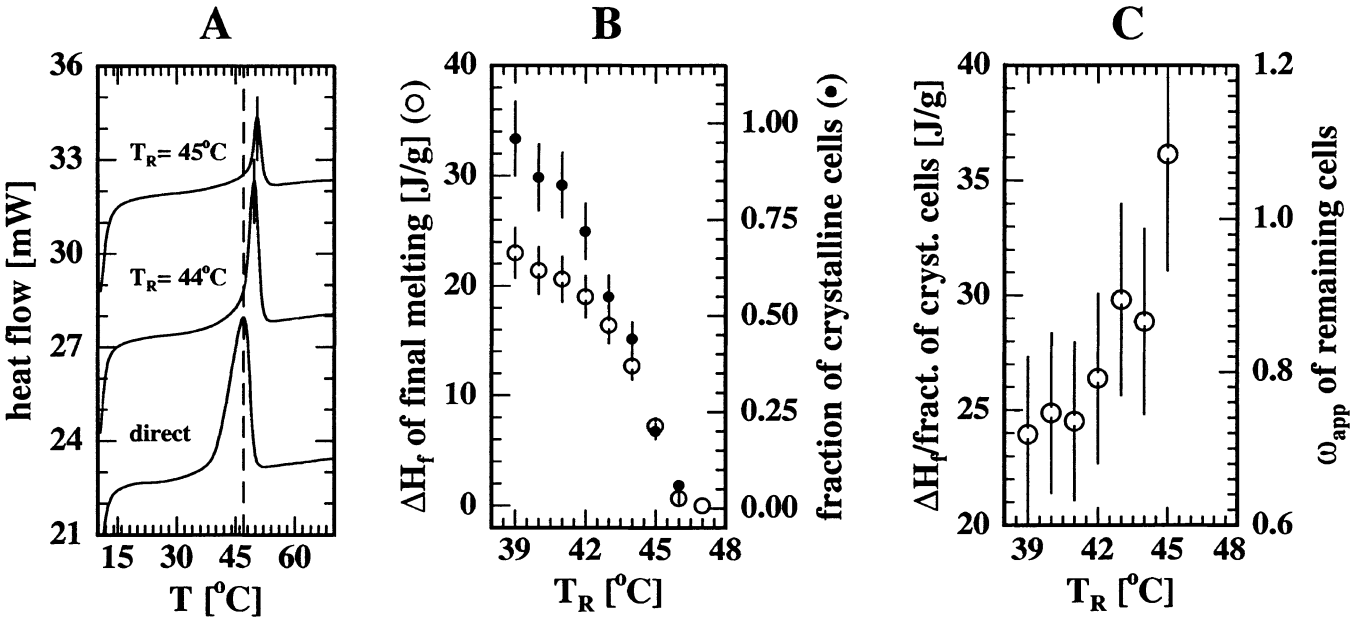

Figure 4. Competing processes of melting and stabilization, as measured by DSC at 10 K/min. (A) Melting after a preceding annealing run up to a temperature T_R as indicated. A melting run measured directly after crystallization is shown for comparison. (B) Heat of melting of remaining crystals ΔH_f obtained from measurements like the one shown in (A) in comparison to the fraction of remaining crystalline cells measured in an AFM experiment on similar sample. (The method used to determine the fraction of molten cells from the AFM data is described in ref 10.) (C) Ratio of the data sets shown in (B), i.e., ΔH_f per fraction of crystalline cells vs the temperature T_R at which partial melting and stabilization took place. This ratio corresponds to an apparent crystallinity ω_{app} of the remaining crystalline cells.

showing a narrowing of Bragg reflections upon reorganization. The lateral size of the crystallites increases during the reorganization process; in addition, thickening of the crystallites might take place.[14]

We now address the melting behavior of these confined nanometer crystals. DSC showed a broad melting range rather than a sharp melting peak (Figure 3). Complementary AFM experiments revealed an explanation for the width of the melting peak:[10] Upon heating a fully crystalline sample to T_R within the melting range, a random pattern of crystalline and amorphous cells appeared. An example is shown in the inset of Figure 1A. This indicates that different cells possess different melting temperatures. We reemphasize that complete melting of individual cells involving enthalpies of several thousand times kT is an irreversible process, excluding the possibility of fluctuations between molten and crystalline states. Consequently, the variation in melting temperatures is *not* caused by thermal fluctuations of small systems.[28] The possibility of a constant temperature "melting−recrystallization" process is also excluded. The different melting temperatures of the individual cells thus reflect the variety of metastable states which are obtained during nucleation, growth, and reorganization.

The difference in stability of the individual nanometer crystals at a given temperature (their degree of order related to their crystallinity) can be probed by a series of two consecutive heating runs. Between these runs the sample is cooled to a lower temperature, e.g., $T = 10$ °C, where no nucleation will yet occur. In the first run the sample was heated to a given temperature T_R located in the melting range. This results in a melting peak corresponding to the cells that were molten during this run. Then, in the second run, the heat of fusion ΔH_f of the remaining cells is measured. Some representative traces of the final heating runs are presented in Figure 4A. With increasing T_R the peak of the endotherm became smaller. Intriguingly, the peak became also narrower and has shifted to higher temperatures, indicating an improved stability of the remaining crystals. Comparing now these results with the number of remaining crystalline cells as obtained from AFM experiments (see Figure 4B), we can clearly identify two independent processes competing for each cell. If the stability of the crystal of an individual cell is too low, it will melt and no crystal will form in this cell during the thermal cycle described above. If the crystal is already sufficiently stable to resist melting, it will not become weaker (less crystalline) but, on the contrary, even improve its stability. Improving crystalline order is facilitated by the larger thermal fluctuations at these rather elevated temperatures allowing for faster rearrangement processes within the crystals. It is only by this combination of AFM and DSC data that we can clearly observe the two opposing trends. On one hand, we have a decrease of the number of crystalline cells with increasing temperature T_R. On the other hand, the remaining cells improve their stability (increase of crystallinity which we express by the increased amount of the heat uptake *per cell* upon melting; see Figure 4C).

Conclusions

In conclusion, as nucleation occurred only at large supercooling, our system allowed a clear temporal separation of growth and reorganization processes. The combination of DSC analysis and AFM allows to identify the different melting temperatures of individual cells as the origin of the broad melting range. Melting of a polymer crystal occurs at a sharply defined temperature and *not* within a range of temperatures. Our results exclude a melting−recrystallization scenario at constant temperature as it is frequently discussed for melting of polymer crystals. The observed broad melting range and the corresponding heterogeneity in thermal stability of the crystals are basic features of the system and do not disappear upon prolonged annealing below the melting range. Although all crystals experienced the same thermal history, they represent different metastable states. It remains an open question how these states are selected and whether this diversity reflects the nontrivial structure present already at the nucleation stage, as has been observed for simple fluids.[29,30]

Acknowledgment. We are grateful to Martina Goldmann for help with the DSC measurements and to Pierre Hoerner and Raffi Krikorian for providing us with the polymer. This work was supported by the EC under Contract HPRN-1999-00151.

References and Notes

(1) Fischer, E. W. *Z. Naturforsch.* **1957**, *12A*, 753.
(2) Keller, A. *Philos. Mag.* **1957**, *2*, 1171.
(3) Strobl, G. R. *The Physics of Polymers*; Springer: Berlin, 1997.
(4) Fischer, E. W. *Kolloid Z. Z. Polym.* **1968**, *263*, 458.
(5) Armistead, K.; Goldbeck-Wood, G. *Adv. Polym. Sci.* **1992**, *100*, 219.
(6) Reiter, G.; Castelein, G.; Sommer, J.-U. *Phys. Rev. Lett.* **2001**, *86*, 5918.
(7) Winkel, A. K.; Hobbs, J. K.; Miles, M. J. *Polymer* **2000**, *41*, 8791.
(8) Al-Hussein, M.; Strobl, G. R. *Eur. Phys. J. E* **2001**, *6*, 305.
(9) Liu, T.; Petermann, J. *Polymer* **2001**, *42*, 6453.
(10) Reiter, G.; Castelein, G.; Sommer, J.-U.; Röttele, A.; Thurn-Albrecht, T. *Phys. Rev. Lett.* **2001**, *87*, 226101.
(11) Ryan, A. J.; Fairclough, J. P. A.; Hamley, I. W.; Mai, S.-M.; Booth, C. *Macromolecules* **1997**, *30*, 1723.
(12) Hamley, I. W. *Adv. Polym. Sci.* **1999**, *148*, 113.
(13) Lotz, B.; Kovacs, A. J. *ACS Polym. Prepr.* **1969**, *10* (2), 820.
(14) Zhu, L.; Chen, Y.; Zhang, A.; Calhoun, B. R.; Chun, M.; Quirk, R. P.; Cheng, S. Z. D.; Hsiao, B. S.; Yeh, F.; Hashimoto, T. *Phys. Rev. B* **1999**, *60*, 10022.
(15) Zhu, L.; et al. *Polymer* **2001**, *42*, 5829.
(16) Loo, Y.-L.; Register, R. A.; Adamson, D. H. *J. Polym. Sci., Part B: Polym. Phys.* **2000**, *38*, 2564.
(17) Loo, Y.-L.; Register, R. A.; Ryan, A. J. *Macromolecules* **2002**, *35*, 2365.
(18) Loo, Y.-L.; Register, R. A.; Ryan, A. J. *Phys. Rev. Lett.* **2000**, *84*, 4120.
(19) Chen, H.-L.; Hsiao, S.-C.; Lin, T.-L.; Yamauchi, K.; Hasegawa, H.; Hashimoto, T. *Macromolecules* **2001**, *34*, 671.
(20) Vonnegut, B. *J. Colloid Sci.* **1948**, *3*, 563.
(21) Balsamo, V.; Paolini, Y.; Ronca, G.; Müller, A. J. *Macromol. Chem. Phys.* **2000**, *201*, 2711.
(22) Hoerner, P.; Riess, G.; Rittig, F.; Fleischer, G. *Macromol. Chem. Phys.* **1998**, *199*, 343.
(23) Strobl, G. R. *Acta Crystallogr., Sect. A* **1970**, *26* 367.
(24) Schwab, M.; Stühn, B. *Phys. Rev. Lett.* **1996**, *76*, 924.
(25) Brandrup, J.; Immergut, E. H. In *Polymer Handbook*, 2nd ed.; Wiley: New York, 1975.
(26) Athas database, http://web.utk.edu/~athas/.
(27) Guinier, A. *X-ray Diffraction in Crystals, Imperfect Crystals, and Amorphous Bodies*; Dover: New York, 1994.
(28) Schmidt, M.; Kusche, R.; Hippler, T.; Donges, J.; Kronmuller, W.; von Issendorff, B.; Haberland, H. *Phys. Rev. Lett.* **2001**, *86*, 1191.
(29) Auer, S.; Frenkel, D. *Nature (London)* **2001**, *409*, 1020.
(30) Matsumoto, M.; Saito, S.; Ohmine, I. *Nature (London)* **2002**, *416*, 409.

MA021434C